D3.6 Report on site-specific risk parameters and stressor indicators

Deliverable number	**D3.6**
Deliverable title	**Report on site-specific risk parameters and stressor indicators**
Nature[1]	**R**
Dissemination Level [2]	**Public**
Author (email) Institution	**Fotios Barmpas (fotisb@auth.gr)** **George Tsegas (gtsegas@auth.gr)** **Eleftherios Chourdakis (chourdakis@auth.gr)**
Editor (email) Institution	**Andreas Papadopoulos (a.papadopoulos@cyric.eu)** **Dimitrios Vamvatsikos (divamva@mail.ntua.gr)**
Leading partner	**AUTh**
Participating partners	**AUTH**
Official submission date:	**30/09/2021**
Actual submission date:	**28/06/2022**

[1] **R**=Document, report; **DEM**=Demonstrator, pilot, prototype; **DEC**=website, patent fillings, videos, etc.; **OTHER**=other

[2] **PU**=Public, **CO**=Confidential, only for members of the consortium (including the Commission Services), **CI**=Classified, as referred to in Commission Decision 2001/844/EC

Modifications Index	
Date	Version
01/03/2022	0.1 Table of content
04/04/2022	0.2 First version
05/05/2022	0.3 Second Version
28/05/2022	0.9 Third Version
01/06/2022	1.0 Final Version

This work is a part of the HYPERION project. HYPERION has received funding from the European Union's Horizon 2020 research and innovation programme under grant agreement no 821054.

Table of Contents

ACRONYMS AND ABBREVIATIONS

CH	Cultural Heritage
CLMcom	Climate Limited-area Modelling Community
CORDEX	Coordinated Regional Climate Downscaling Experiment
DSS	Decision Support System
ECA&D	European Climate Assessment & Dataset
ETCCDI	Expert Team on Climate Change Detection and Indices
GCM	Global Climate Model
GEV	Generalized Extreme Value
GP	Generalised Pareto
HadGEM2-ES	Hadley Centre Global Environmental Model 2 - Earth System
HT	Hygro-Thermal
ICHEC	Irish Center for High-End Computing
KNMI	Koninklijk Nederlands Meteorologisch Instituut
MOHC	Met Office Hadley Center
MPI-ESM-LR	Max Planck Institute Earth System Model Low Resolution
MPI-M	Max Planck Institute for Meteorology
POT	peaks-over-threshold
RCA4	Rossby Centre regional atmospheric model 4
RCM	Regional Climate Model
RT	Real Time
SMHI	Swedish Meteorological and Hydrological Institute
WMO	World Meteorological Organization

WP	Work Package

List of Tables

List of Figures

Executive Summary

This deliverable aims to provide a detailed description of the qualitative and quantitative assessment on the relevance of primary and secondary impact indicators derived from climate calculations and RT in-situ measurements. These indicators will followingly be used in WP5-WP7 as input in the process of providing RT hazard assessments for the DSS, as well as HT and structural vulnerability assessment. The data used in the analysis described in the frame of this document originated from the EURO-CORDEX project, exploiting multiple RCM simulations performed by different GCMs to cover the period from 1971 to 2100. The variables considered in this analysis comprise ambient temperature and precipitation.

1. Introduction

1.1 Purpose and Scope

This document is an outcome of Task 3.6 “Assessment of primary and secondary site-specific climate risk parameters and atmospheric stressor indicators” towards the collection and assessment of the relevance of primary and secondary impact indicators derived from climate calculations and real time in-situ measurements. This deliverable focuses on the methods, approaches and techniques utilized in order to prepare and deliver a set of appropriate indicators for climate impacts on the overall areas of the CH structures in the pilots.

1.2 General Idea

The general idea for the present approach is based on the analysis of climate impacts conducted for the the four CH pilot areas of the Project, namely Rhodes, Granada, Venice and Tonsgberg. The obtained information will be employed in determining site-specific harshness criteria as regards climate stressors. The meteorological parameters used in the framework of the present analysis are the ambient temperature and the precipitation. Additional variables, such as relative humidity, wind speed and wind direction will be employed for the overall analysis of the pilot sites, using the same techniques presented herein.

2. Methodology and Input Data

2.1 Descriptive indices of extremes

Aiming to obtain a uniform perspective on observed changes in weather and climate extremes, ETCCDI has defined a core set of descriptive indices of extremes (Klein Tank et al., 2009). The indices describe specific characteristics of severes, including frequency, amplitude and persistence. More specifically, the core set consists of 27 extremes indices as regards ambient temperature and precipitation and is widely used as a tool to estimate and inspect variations in extremes (Peterson and Manton, 2008; Alexander et al., 2006).

Metrics for assessing the ability of global and regional climate models to simulate moderate extremes are provided, as well. Projected differences in these indices are revealing of future climate change in extremes. Utilizing similar characterizations of extremes and analysing the corresponding data in a standardized way provides the capability of comparing results referring to different areas and to obtain consistent pictures of change around the world (Klein Tank et al., 2009).

Besides the aforementioned core set of indices, additional extremes indices can be defined in order to meet the more specific adaptation needs in certain regions. For example, the ECA&D project defined 13 additional indices focusing explicitly on temperature extremes. Participants at the ETCCDI workshop held in South East Asia indicated that additional precipitation indices could be used to describe the onset and

ending dates of the monsoon season. The indices concept allows for such additional definitions, which become particularly relevant if they are calculated in a standardized way for several countries in a region (Klein Tank et al., 2009).

2.2 Statistical modelling of extremes

The illustrative indices developed by ETCCDI refer to modest extremes occuring systematically during a typical year. Extreme value theory (Coles, 2001; Smith, 2002; Katz et al., 2002) enhances the descriptive indices in the process of evaluating the intensity and frequency of rare events which could be characterized as outliers of weather variables. More specifically, this theory is related to events occuring once in 20 years or rarer.

In some engineering approaches, the application of an analysis like that demands the assessment of events that are unprecedented in the available record, as they take place once in a hundred or thousand years (extreme quantiles of the statistical distribution), while the available observational timeseries may contain data for a 50 year period (Klein Tank et al., 2009). The most common approach implies the fitting of a statistical model to the annual extremes in a certain timeseries of available data. WMO provides an extensive review of probability distributions and methodologies for the assessment of their parameters (WMO, 1989).

Overall, the extreme quantiles of interest are extracted from an extreme value distribution using two general methods, namely the peaks-over-threshold (POT) method and the block maximum approach. More specifically, the POT method is employed to denote the behaviour of exceedances above a high threshold, as well as the threshold crossing process. Under favourable conditions, and using a high enough threshold, extremes identified by this approach will have a generalized Pareto (GP) distribution (Smith, 2002).

In general, despite the fact that the successful execution of the POT method requires more decisions from the user (manual declustering of extremes, specification of a sufficiently high threshold, etc.) than the block maximum approach, it provides the capability of using the information available in the observed dataseries in a more efficient way (Kharin et al., 2007). As a result, the application of POT method could result in more accurate estimates of extreme quantiles.

On the other hand, the block maximum method constitutes a more generally used method, which is based on an explicit extreme value theory. In the frame of this methodology, the user considers the sample of extreme values acquired by selecting the maximum or the minimum (depending on the specific characteristics of each application) value observed in each block. Typical blocks consist of yearly timeseries with a temporal resolution of one day and, occasionally, seasonal timeseries (for example, the maximum temperature during summertime or the minimum wintertime temperature).

Statistical theory signifies that the Generalized Extreme Value (GEV) distribution is the most appropriate approach for the estimation of the block maxima when blocks are sufficiently large. In its general form, the GEV distribution consists of three parameters, more specifically the location, the scale and the shape. These parameters can be assessed using a set of different methodologies such as the method of maximum likelihood (Jenkinson, 1955), the method of L-moments (Hosking, 1990) or the ordinary method of moments. The maximum likelihood approach is preferred when samples of extremes are sufficiently large, as well as in cases wherethe climate may not be stationary. In such cases, the maximum likelihood method could include "covariates" so as to integrate the impacts of nonstationarity on extremes (Klein Tank et al., 2009).

On the other hand, the method of L-moments is mostly used when the samples are small, as in these cases the estimation of the parameters of the GEV distribution using the maximum likelihood is not always successful (Kharin and Zwiers, 2005). The ordinary method of moments, in which the mean, variance and skewness of the sample of extremes are matched to theoretical expressions for the mean, variance and skewness of the GEV distribution is not recommended, as it tends to underestimate long-period return values (Landwehr et al., 1979).

In this point, it should be noted that it is a matter of major importance to validate the data fit of the produced distribution (Kharin and Zwiers, 2000) and to determine the uncertainty of the estimates of the distribution's parameters by calculating appropriate standard errors and confidence intervals. The latter can be achieved rather easily if the maximum likelihood method has been applied, as the statistical theory offers expressions that generally provide fairly good approximations for these quantities.

In order to achieve further evaluation of the produced results, comparing the parametric estimates of quantiles for moderate return periods could be compared to the corresponding empirical estimates. This approach could assist the identification of the major factors of uncertainty, which may be related to the statistical techniques, but are for sure dependent on the sample characteristics.

A problem that comes up in this context is handling outliers that have been retained after thorough quality control, evaluation of available metadata and assessment of corroborating information such as published media reports. Such outliers, which could be much larger than any other observation in the record, signify well-documented events in which the specific observation is not in doubt, with respect to the supporting metadata and other information. In cases like that, the analyst may find that the fitted distribution is very sensitive to the inclusion or exclusion of the outlier, and goodness-of-fit statistics may indicate that the quality of the fit is reduced by its inclusion (Klein Tank et al., 2009).

Moreover, it is often the situation in such cases that if the outlier is excluded, estimated return values for return periods corresponding to the length of the record

are smaller than the outlying observation. While there is a clear evidence that the chosen extreme value distribution does not fully depict the whole of the available reliable observations, it would be prudent to incorporate the outlier in the analysis and to take into account the possibility that return value estimates and corresponding confidence intervals may be subject to some error. Ignoring a well-documented extreme observation in the record to obtain an apparently better statistical fit would evidently generate inaccurate return value estimates, given the evidence embodied by the outlying extreme. As a result, it is not recommended.

In addition to assessing goodness-of-fit by using a standard evaluation statistic or by examining a quantile-quantile plot, it is also important to estimate the feasibility of the generated distribution. More specifically, the analyst should examine whether the whole set of the observed extremes is possible under the fitted distribution (Dupuis and Tsao, 1998; Kharin and Zwiers, 2000). In the case of the GEV distribution, the shape parameter verifies if the fitted distribution will have a finite lower bound, a finite upper bound, or no bound at all. In the unbounded case, the shape parameter is set to zero, and the GEV distribution transforms to the Gumbel distribution (Gumbel, 1958), which has been used extensively in hydrology, meteorology and engineering.

In cases in which the fitting procedure results in a non-zero estimate of the shape parameter, it is essential to ensure that all observed extremes lie either to the right of the lower bound of the produced distribution when the shape parameter is estimated to be positive or to the left of the upper bound of the fitted distribution when the shape parameter is estimated to be negative. If the fitted distribution is infeasible, that is, if it would be impossible for one of the observed extremes to occur under the fitted distribution, then the estimated shape parameter should be fine-tuned to enforce feasibility (Dupuis and Tsao, 1998). Van den Brink and Können (2008) illustrate a certain methodology which can be used to identify the influence of outliers by assessing the statistical distribution of all outliers in several timeseries in a specific area or in a combination of corresponding data.

The extreme value theory that underlies the GP and GEV distributions requires assumptions such as stationarity. Although considerably long period return values can be estimated by the produced distribution, the confidence that can be placed in the results may be minimal if the length of the return period is considerably longer than the period covered by the sample of extremes. Estimating return levels for extensive return periods is disposed to large sampling errors and potentially large biases because of the inaccurate understanding of the shape of the tails of the distribution. In general, confidence in a return level decreases rapidly when the period becomes larger than two times the length of the original data set (Klein Tank et al., 2009).

A final point of concern before the actual application of the methodology is related to the interpretation of estimated return values. In the case of a stationary climate, return values have a clear interpretation as the value that is expected to be exceeded on average, once every return period, or with probability 1/(return period) in any given year. On the other hand, in the case of a changing climate, return values can

have several different interpretations. More specifically, one possibility is to estimate a level such that the probability of exceedance is currently 1/(return period). In this case, a suitable interpretation for the return value would be that if similar estimates were made at many different places, then one would expect exceedances to occur at about 100/(return period) percent of locations, that is, the return value/return period pair gives an indication of the current risk of an extreme event with magnitude at least as large as the return value.

Another possibility would be to use a prediction of future climate change to estimate a level such that the probability of exceedance in any one year is never greater than 1/(return period) over a fixed period, such as between the present and year 2200. Given that the risk of exceedance would likely be increasing with time, the objective in this case would be to estimate the level for which the probability of exceedance would be 1/(return period) in the last year of the period of interest.

Moreover, a third possibility would be to again use a projection of climate change, but in this case to estimate the appropriate level so that the average probability of exceedance over a fixed period, such as from the present to year 2200, is 1/(return period). In this case, the probability of exceedance would be less than 1/(return period) during the initial years of the period of interest but greater than 1/(return period) during the later years of the period. This third analysis could potentially be suitable in cases in which the lifetime risk of failure due to an extreme event of a planned piece of infrastructure is considered (Klein Tank et al., 2009).

2.3 ETCCDI indices

The core set of the 27 descriptive indices of extremes defined by the Joint CCl/CLIVAR/JCOMM Expert Team on Climate Change Detection and Indices (ETCCDI; URL1) are separated into two distinctive categories, more specifically those related to ambient temperature and those referring to precipitation. Out of the full set of 27 indicators, only the following eight indicators provide information relevant to the application in CH sites:

1. FD: Frost Days
2. ID: Icing Days
3. TN10p: Cold Nights
4. TN90p: Warm Nights
5. DTR: Diurnal Temperature Range
6. Rx5day: Maximum five-day Precipitation
7. R95pTOT: Precipitation due to Very Wet Days
8. R99pTOT: Precipitation due to Extremely Wet Days

Brief definitions of the aforementioned indices are provided followingly.

Temperature indices

- **FD (frost days):** count of days where TN (daily minimum temperature) < 0 C:

Calculation steps: Let TN_{ij} be the daily minimum temperature on day *i* in period *j*. Count the number of days where TN_{ij} <0 C.

- **ID (icing days):** count of days where TX < 0 C

Calculation steps: Let TX_{ij} be the daily maximum temperature on day *i* in period *j*. Count the number of days where TX_{ij} < 0 C.

- **$TN10_p$ (cold nights):** count of days where TN < 10^{th} percentile

Calculation steps: Let TN_{ij} be the daily minimum temperature on day *i* in period *j* and let TN_{in10} be the calendar day 10^{th} percentile of daily minimum temperature calculated for a five-day window centred on each calendar day in the base period *n* (1961-1990). Count the number of days where $TN_{ij} < TN_{in10}$.

- **$TN90_p$ (warm nights):** count of days where TN > 90^{th} percentile

Calculation steps: Let TN_{ij} be the daily minimum temperature on day *i* in period *j* and let TN_{in90} be the calendar day 90^{th} percentile of daily minimum temperature calculated for a five-day window centred on each calendar day in the base period *n* (1961-1990). Count the number of days where $TN_{ij} > TN_{in90}$.

- **DTR (diurnal temperature range):** mean difference between TX and TN (C)

Calculation steps: Let TX_{ij} and TN_{ij} be the daily maximum and minium temperature on day *i* in period *j*. If *I* represents the total number of days in *j* then the mean diurnal temperature range in period *j* is DTR_j = sum (TX_{ij} - TN_{ij})/*I*.

Precipitation indices

- **RX5day (maximum five-day precipitation):** highest precipitation amount in five-day period:

Calculation steps: Let RR_{kj} be the precipitation amount for the five-day interval *k* in period *j*, where *k* is defined by the last day. The maximum five-day values for period *j* are RX_{5dayj} = max (RR_{kj}).

- **R95pTOT:** precipitation due to very wet days (> 95^{th} percentile)

Calculation steps: Let RR_{wj} be the daily precipitation amount on a wet day *w* (RR ≥ 1 mm) in period *j* and let RR_{wn95} be the 95^{th} percentile of precipitation on wet days in the base period *n* (1961-1990). Then $R95pTOT_j$ = sum (RR_{wj}), where $RR_{wj} > RR_{wn95}$.

- **R99pTOT:** precipitation due to extremely wet days (> 99^{th} percentile)

Calculation steps: Let RR_{wj} be the daily precipitation amount on a wet day *w* (RR ≥ 1 mm) in period *j* and let RR_{wn99} be the 99^{th} percentile of precipitation on wet days in the base period *n* (1961-1990). Then $R99_{pTOTj}$ = sum (RR_{wj}), where $RR_{wj} > RR_{wn99}$.

At this point, it should be noted that the typical length of the periods *j* is one year. Nevertheless, it is possible that different period lengths (such as seasonal) could fit better in the specific characteristics of certain regions under investigation. Besides, the values of the percentile thresholds are determined empirically from the observed station series in the climatological standard normal period 1961–1990, but the choice of another normal period (e.g. 1971–2000 or 1981-2000) can lead to slight impacts on the results as regards the changes in the indices over time (Klein Tank et al., 2009).

The percentiles used are extracted from five-day windows centred on each calendar day to account for the mean annual cycle. A five-day window is chosen to yield a total sample size of 30 years × 5 days = 150 for each calendar day, which results in a relatively smooth annual cycle of percentile thresholds. This approach ensures that extreme temperature events, in terms of exceedings of percentile thresholds, can occur with equal probability throughout the year. The bootstrap procedure of Zhang et al. (2005) has been implemented to ensure that the percentile-based indices do not have artificial jumps at the boundaries of the base period.

2.4 Input Data

The climate data used in the frame of the present analysis originated from the EURO-CORDEX archive (Kotlarski et al., 2015) with a spatial resolution of 0.11° (~12.5 km) and a daily temporal resolution. For each of the four areas under investigation (Rhodes, Granada, Venice and Tonsberg), the single grid point closest to the site was utilized in terms of better representativity of the typical meteorological conditions occuring in the particular area of interest. Based on the sensitivity analysis perfomed in Deliverable D3.1, where several RCM simulations driven with lateral boundary conditions from different GCM runs were analyzed, the scenario RCP4.5 was examined, representing the central of the available scenarios in terms of emissions and radiative forcing (van Vuuren et al., 2011).

The RCP4.5 scenario stands for a world in which relatively well-succeeded mitigation of greenhouse gas emissions occurs. In the frame of this particular scenario, the radiative forcing stabilizes at 4.5 W m^{-2} relative to preindustrial conditions in the year 2100 without ever exceeding that value.

In this point it should be noted that the analyzed climate model simulations cover the period extending from 1971 to 2100. The selection of these simulations was based on the data availability for the required variables under all the three RCP scenarios. The variables used in this application contain the daily maximum and minimum near-surface (2 m height) ambient temperatures, the cummulative daily precipitation, the daily maximum sustained wind speed (10 min average of wind speed at a 10 m height) and the daily means of eastward and northward wind components at 10 m height. The scenario model runs beginning from 2006 were merged with the historical model runs ending in 2005. Hence, the period 1971–2005 is identical in different RCP scenarios.

Analysis was conducted for a GCM model run driven by the MPI-M-MPI-ESM-LR model (Stevens et al., 2013) and downscaled by the SMHI-RCA4 model.

As regards the site-specific meteorological risks, slightly different parameters were analysed for each area under investigation. Changing freeze and thaw cycles were recognised as a threat in every location. As a result, the number of days with ambient temperature at 2 meters above the ground crossing the interval from -1 °C to +1 °C was analysed at each site. Moreover, as Venice was additionally recognised to be very vulnerable to the extreme cold, the number of days with minimum temperature below -5 °C were also counted during the most severe cold spells temperature dropping below -5 °C.

Along with alternating freeze and thaw cycles, heavy precipitation leading to flash floods or longer periods with abundant rain pose a risk to every site. Therefore, the days with heavy precipitation and 5-day periods with highest precipitation amounts were detected, similarly at each site. In Venice, heavy rain is particularly problematic if strong southeasterly winds blowing from the Adriatic Sea raise the sea level concurrently. As a result, in this particular site, projected changes in strong southeasterly winds and detected combined occurrences of heavy precipitation and strong southeasterly wind were analysed as well. Generally, strong winds were recognized as a threat for Rhodes and Tonsberg. As a consequence, projected changes in strong wind speeds were analysed in these locations.

For 1-day and 5-day precipitation amounts, as well as for elevated wind speeds, return levels were initially computed from the four ERA-Interim driven model calculations. These return levels were subsequently used in the establishment of thresholds for episodic events. For the cases of 1-day and 5-day precipitation sums, two distinct threshold values were selected. The lower of them were arranged in a low level, aiming so as they can be exceeded on several days per year at each site, on average. In this way, there was no need for setting site-specific thresholds, as there is a large number of events for all sites based on the lower thresholds used.

Return levels for heavy precipitation events and strong winds (rr_return_levels, ws_return_levels and se_wind_return_levels) are calculated for the 30-year periods 1971–2010, 2011–2040, 2041–2070 and 2071–2100.

3. Results

3.1 Granada

The site of Granada is placed in the southern part of Spain at an average altitude of about 700 m above sea level. Despite the fact that Granada is located fairly close to the sea, freeze-thaw cycles can regularly be noticed due to the aforementioned high terrain elevation.

During heavy precipitation simulations different RCMs generate quite diverse results in Granada (see HYPERION D3.1). Normally, precipitation levels projections in the Mediterranean region depict a decrease due to global warming, but as also in the case

of Rhodes in Granada this is reflected mainly due to lower thresholds and short return levels.

Table 1 summarizes the temperature-related indicators for the site of Granada. TN10p and TN90p are calculated using a five-year bootstrap process. The most prominent trend visible in the future under the RCP4.5 scenario is the reduction of frost days, while the number of icing days remains zero. TN10p and TN90p do not reveal any significant trend on the nighttime temperatures. The daily temperature range is slightly decreasing over the simulated period, but the most important feature is a small but consistent increase in the variation predicted towards the end of the century, as evident in the monthly DTR series shown in Figure 1. This indicates an increased predicted intra- and inter-annual variability, mainly due to an increased frequency of small DTR values.

Table 1: ETCCDI Temperature-related Indicators for the site of Granada

Period	FD	ID	TN10p	TN90p	DTR (degrees)
1971–2010	79	0	14.80866	11.0746	10.56149
2011–2040	46	0	11.25345	16.49533	10.50557
2041–2070	48	0	12.80159	14.15987	10.46259
2071–2100	31	0	12.50952	14.15657	10.39858

In Table 2, the Precipitation-related indicators are presented. R95pTOT and R99pTOT are calculated using a five-year bootstrap process. RX5day stabilizes after 2011 and does not imply any increase in precipitation extremes. R95pTOT does not excibit any clear long-term trend, revealing a stable contribution of very rainy days in the total precipitation. The contribution of extremely rainy days, however, shows a slight increase towards the end of the century, as indicated by values of R99pTOT. Looking at the corresponding timeseries of yearly averages (Figure 5), the trend stabilizes at the beginning of the millennium and shows little variation henceforth.

Table 2: ETCCDI Precipitation-related Indicators for the site of Granada

Period	RX5day (mm)	R95pTOT (mm)	R99pTOT (mm)
1971–2010	37	469.2123	180.6976
2011–2040	43	435.1328	190.9671
2041–2070	56	486.0722	216.0503
2071–2100	45	431.8231	194.8082

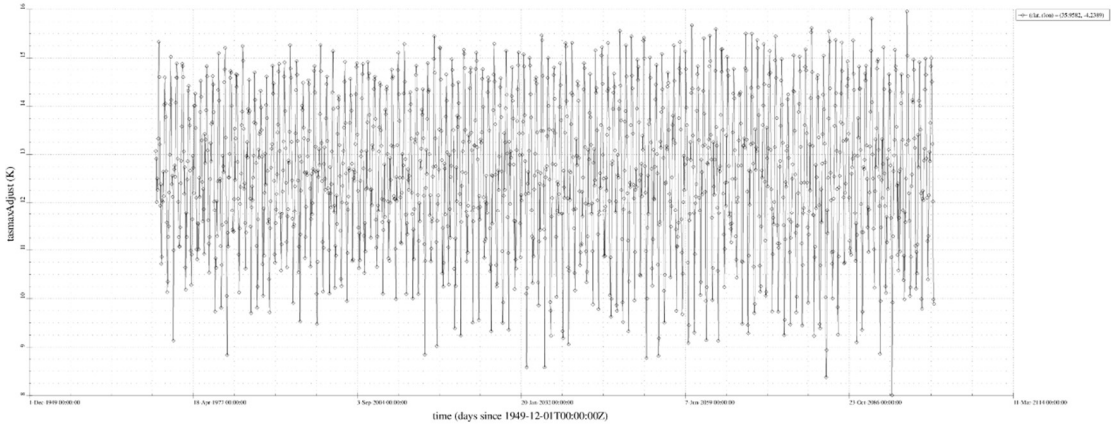

Figure 1: Time series of monthly DTR for the site of Granada.

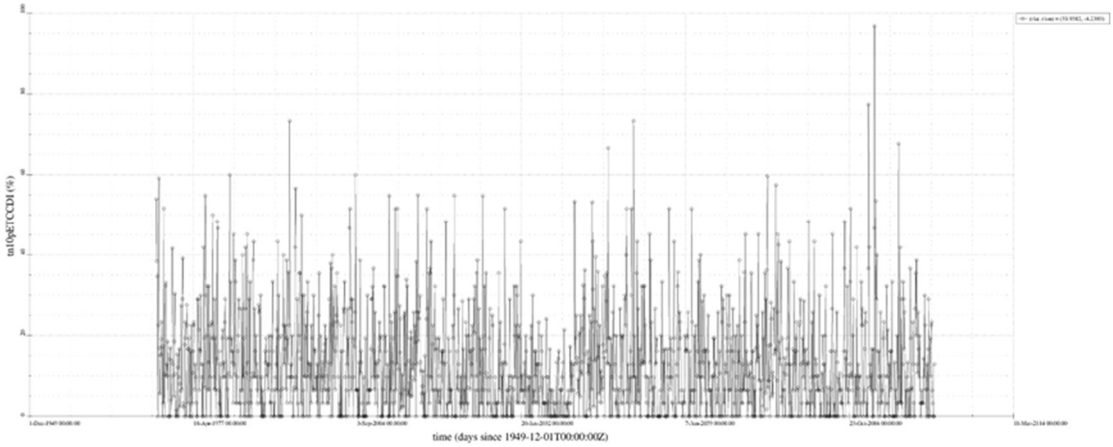

Figure 2: Time series of monthly TN10p for the site of Granada.

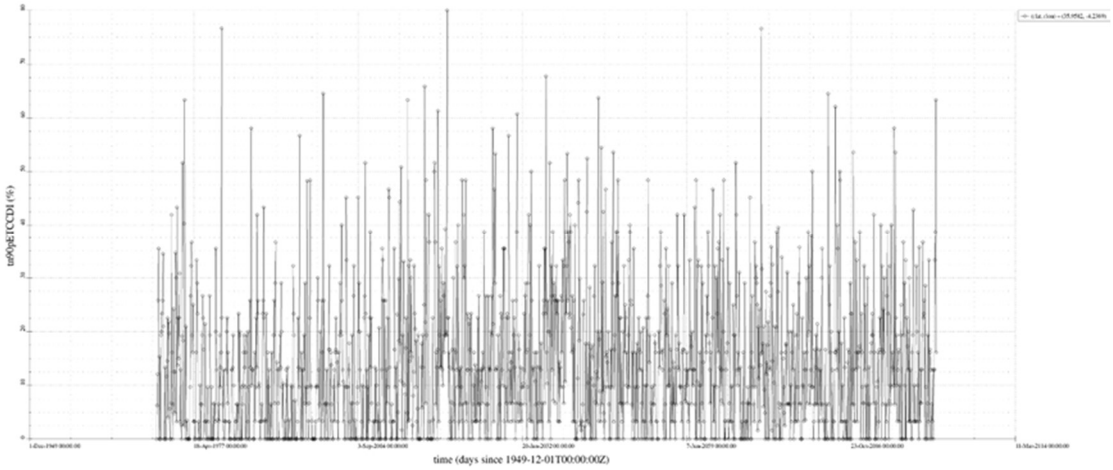

Figure 3: Time series of monthly TN90p for the site of Granada.

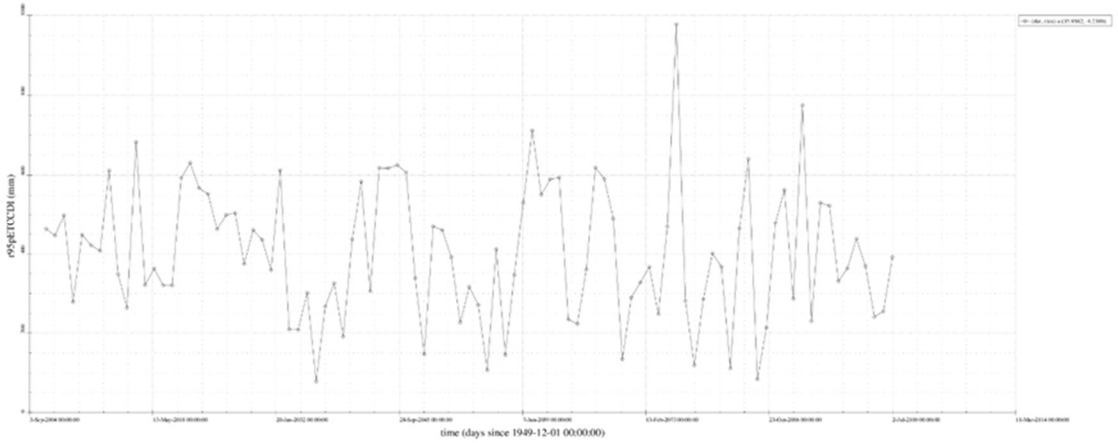

Figure 4: Time series of annual R95pTOT for the site of Granada.

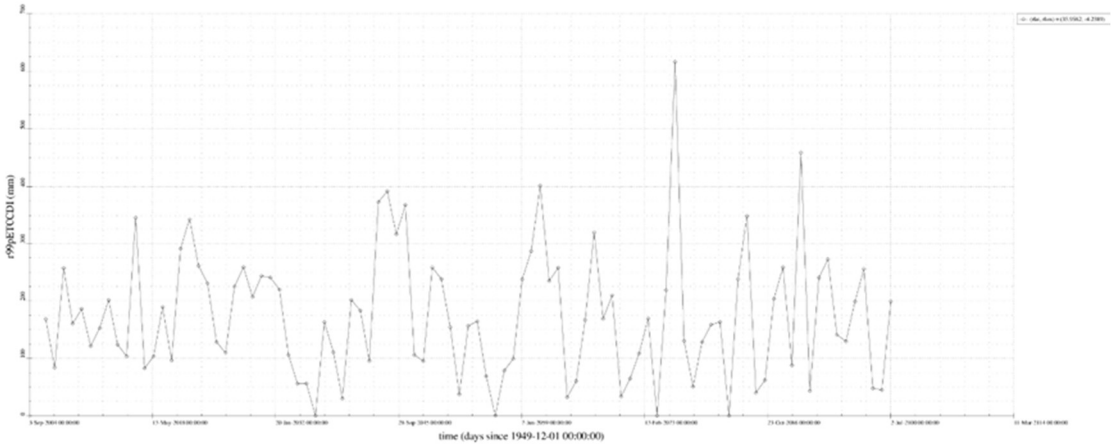

Figure 5: Time series of annual R99pTOT for the site of Granada.

3.2 Rhodes

As regards the case study of Rhodes, it is the largest of the Dodecanese islands and is located in the Mediterranean Sea. Because of the vicinity of the sea, freezing temperatures in Rhodes are extremely rare.

Future scenarios are not related to significant change in the occurrence of heavy precipitation in Rhodes. The temperature-related indicators as listed in Table 3 reveal a consistently vanishing number of Frost- and Icing days, while the nighttime temperature trends, as measured by TN10p and TN90p, do not excibit any clear long-term trend. The diurnal temperature range mean values (DTR) also remain constant throughout the simulation period, and no discernible pattern can be seen in the corresponding time series of monthly values (Figure 6).

Table 3: ETCCDI Temperature-related Indicators for the site of Rhodes

Period	FD	ID	TN10p	TN90p	DTR (degrees)
1971–2010	7	0	14.35486	15.41101	6.198909
2011–2040	0	0	13.06329	14.5793	6.213999
2041–2070	2	0	9.355618	18.97849	6.140188
2071–2100	0	0	12.16522	15.74174	6.119838

Period averages of precipitation-related indicators are presented in Table 4, where as stated before, R95pTOT and R99pTOT are calculated using a five-year bootstrap process. RX5day is relatively constant for the two middle periods, but decreases significantly after 2071, indicating less frequent seasonal episodes of contiguous rainy days. Both R95pTOT (contribution of very rainy days) and R99pTOT (contribution of extremely rainy days) do not excibit any clear long-term trend until 1970, however they are both significantly reduced during the last part of the century. Looking at the corresponding timeseries of yearly averages (Figures 9 and 10), this trend is evident near the end of the millennium while interannual variation of the indicators remains unchanged compared to previous periods.

Table 4: ETCCDI Precipitation-related Indicators for the site of Rhodes

Period	RX5day (mm)	R95pTOT (mm)	R99pTOT (mm)
1971–2010	47	522.1486	179.5029
2011–2040	48	571.4655	196.0085
2041–2070	49	557.5575	191.5823
2071–2100	32	466.8386	184.2696

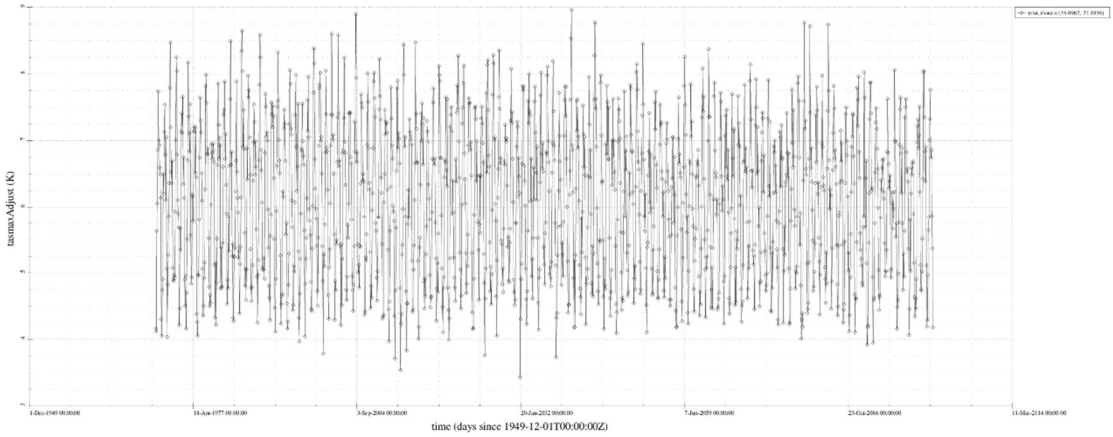

Figure 6: Time series of monthly DTR for the site of Rhodes.

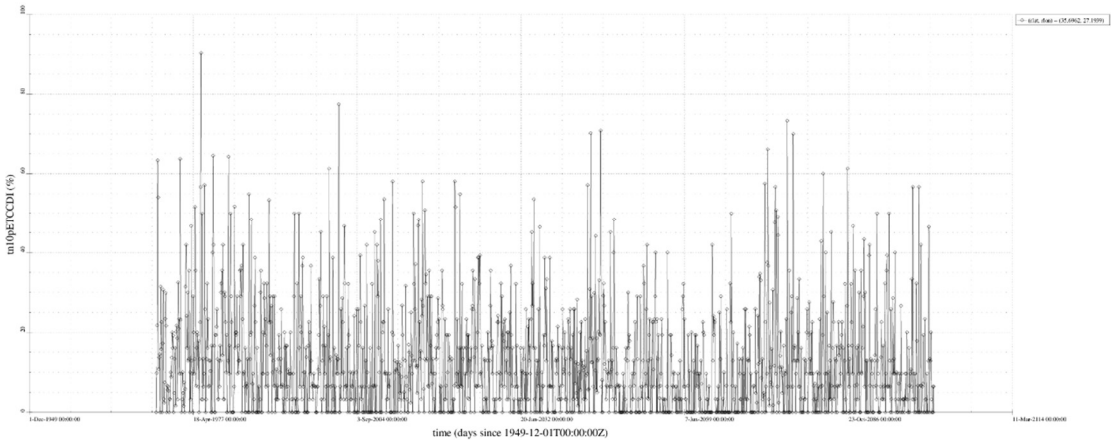

Figure 7: Time series of monthly TN10p for the site of Rhodes.

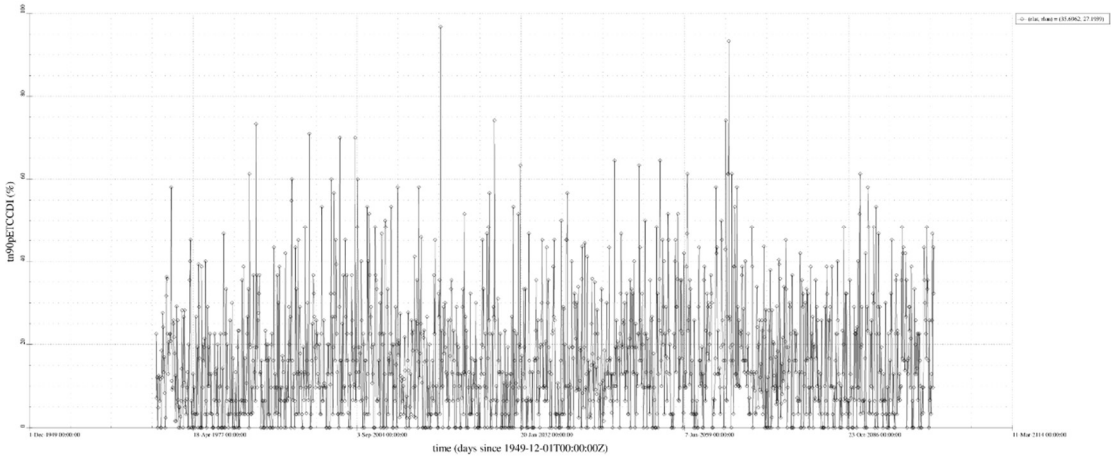

Figure 8: Time series of monthly TN90p for the site of Rhodes.

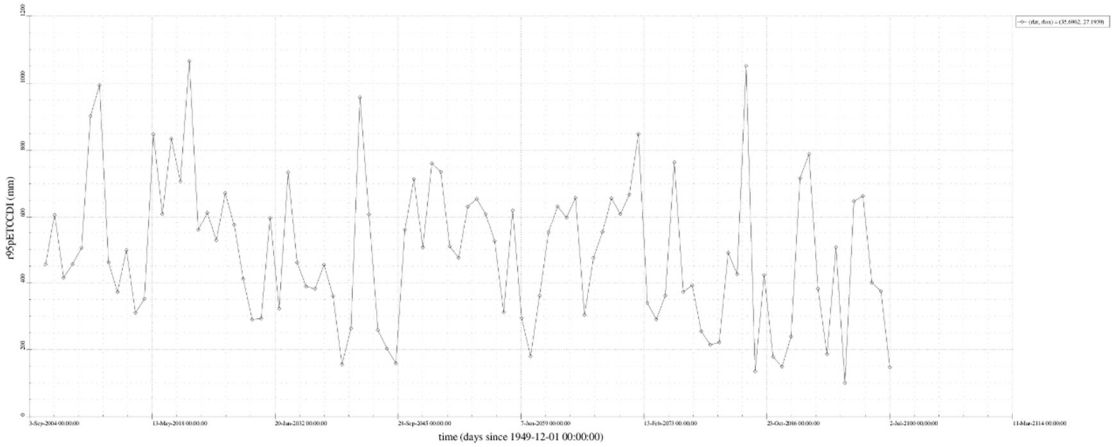

Figure 9: Time series of annual R95pTOT for the site of Rhodes.

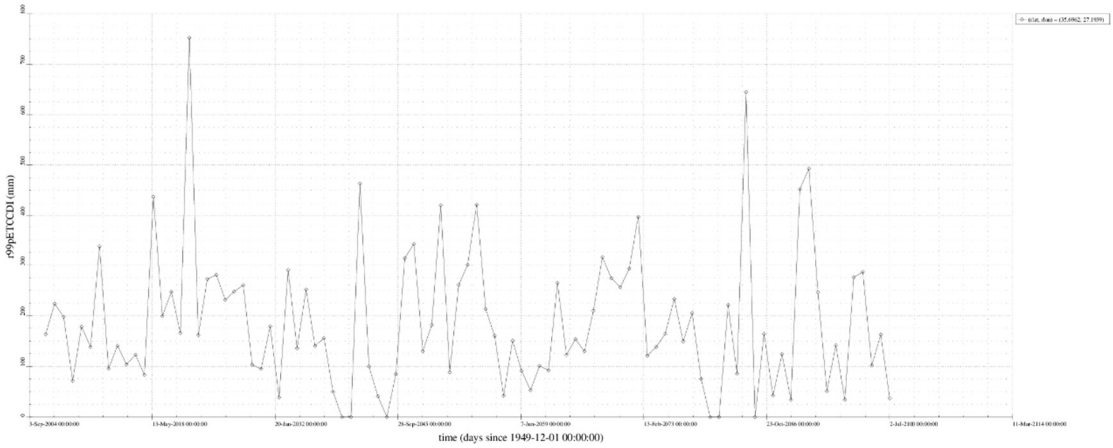

Figure 10: Time series of annual R99pTOT for the site of Rhodes.

3.3 Venice

Venice is a city located in the northern shore of the Adriatic Sea. In general, due to its location its climate tends to be cooler than in Granada and Rhodes. As a result, freeze-thaw cycles in Venice are experienced more commonly than in the other pilot Mediterranean sites. The variability in the frequency of freeze-thaw cycles among the RCM simulations in Venice is rather similar to the one in Granada.

Venice is particularly vulnerable to flooding when heavy precipitation occurs together with unfavourable wind conditions, which was analyzed in the framework of Deliverable D3.1.

The calculated Temperature-related indicators calculated under the RCP4.5 scenario are tabulated in Table 5. The most important trend revealed here is the reduction of predicted frost days almost to a third, compared to the 1971-2010 period, and the corresponding elimination of icing days. The implications of this predicted change is a reduction in the freezing-thawing cycles underwent by assets and possible biological effects on the behaviour and consistency of microflora growth on surfaces. Nighttime temperature indicators reveal little change over the simulation period, where only TN90p (percentage of warm nights) exhibits a reduction in the last period (2071-2100). Calculated diurnal temperature range (DTR) shows little variation in terms of period averages, but looking at the monthly variation (Figure 11) a clear trend of increasing variability is evident as the time progresses, indicating unstable and potentially unpredictable behaviour of diurnal temperature cycles even though the averages remain constant.

Table 5: ETCCDI Temperature-related Indicators for the site of Venice

Period	FD	ID	TN10p	TN90p	DTR (degrees)
1971–2010	989	26	14.90511	12.58036	7.224822
2011–2040	540	17	15.71696	17.71528	7.257175
2041–2070	513	8	11.56113	19.57794	7.344915
2071–2100	270	3	13.94924	13.33437	7.291243

Table 6 summarizes the period means of calculated Precipitation-related indicators for the site of Venice. Both the extreme indicators (R95pTOT and R99pTOT) show a consistent increase of very wet days and extremely wet days contribution, throughout

the simulation period. This indicates a clear trend of more frequent days of concentrated extreme precipitation, which can contribute to an increased flash-flooding risk. The inter-annual variability of the corresponding indicators remains unchanged throughout the simulation period. Precipitation due to consecutive rainy days, as indicated by RX5day also remains unchanged during the simulation period.

Table 6: ETCCDI Precipitation-related Indicators for the site of Venice

Period	RX5day (mm)	R95pTOT (mm)	R99pTOT (mm)
1971–2010	29	416.651	154.1324
2011–2040	32	438.5461	164.7228
2041–2070	30	468.1178	173.8889
2071–2100	32	477.1623	175.6597

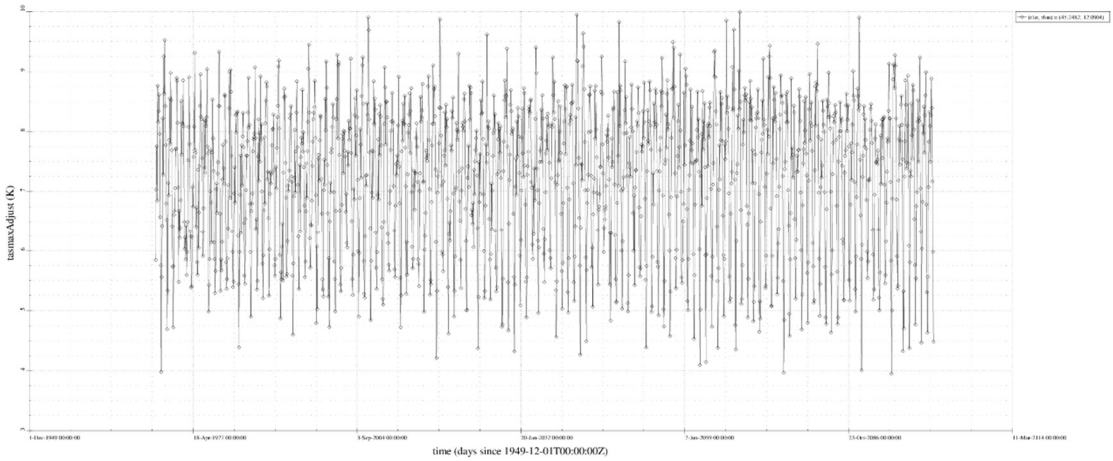

Figure 11: Time series of monthly DTR for the site of Venice.

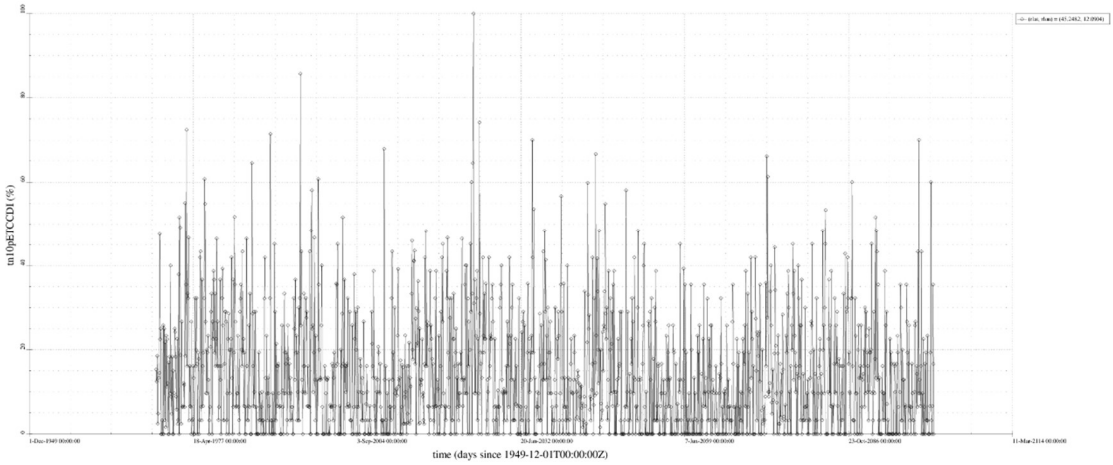

Figure 12: Time series of monthly TN10p for the site of Venice.

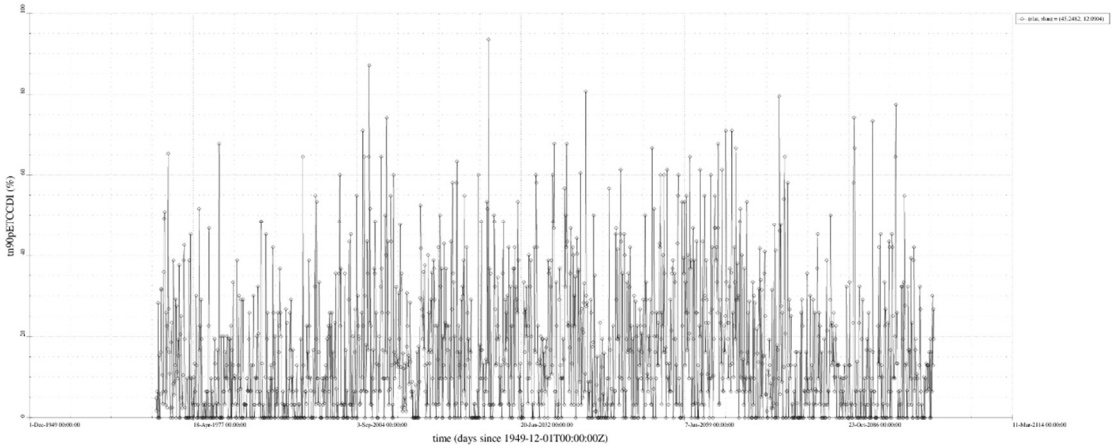

Figure 13: Time series of monthly TN90p for the site of Venice.

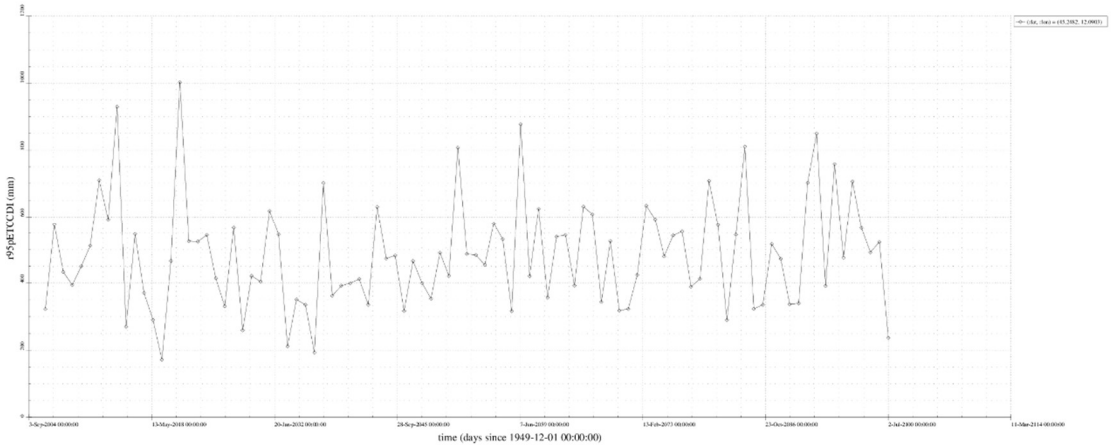

Figure 14: Time series of annual R95pTOT for the site of Venice.

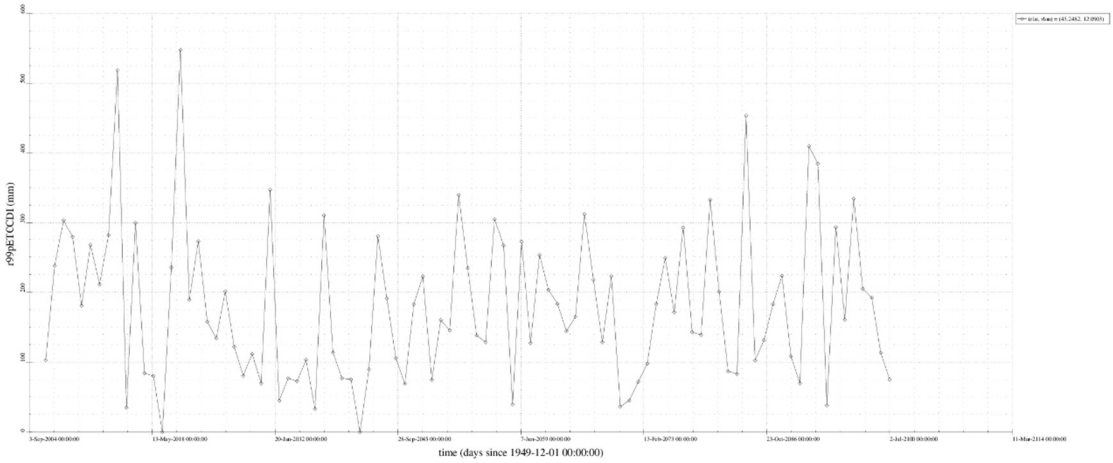

Figure 15: Time series of annual R99pTOT for the site of Venice.

3.4 Tonsberg

Tonsberg is located in the southern part of Norway and has a quite different climate relative to the rest of the sites under investigation that are situated around the shores of the Mediterranean Sea. As a result, freeze-thaw cycles occur in Tonsberg rather frequently, especially in contrast to the other areas of interest. Nevertheless, their frequency varies among the model simulations in a similar way as in Venice (HYPERION D3.1). Besides, in this case global warming tends to lead to a decreasing occurrence of freeze-thaw cycles.

In Table 7 period averages of the Temperature-related indicators are shown. The most important trend is of course the reduction in frost days (almost halving) and icing days (almost to a third) compared to the 1971-2010 period. On the other hand, the nighttime temperature indicators TN90p and TN10p do reveal an accompanying trend of more cold nights and less warm ones, at least for the last part of the century. Average values of the projected diurnal temperature range do not significantly change over the whole simulated period, nevertheless looking at the corresponding time series (Figure 16) it is evident that low-DTR months increase in time, indicating longer-running spells of cloudy days (as well as very warm days) where DTR typically exhibits its minima.

Table 7: ETCCDI Temperature-related Indicators for the site of Tonsberg

Period	FD	ID	TN10p	TN90p	DTR
1971–2010	4818	1726	13.28775	15.76203	7.601521
2011–2040	3271	1108	12.97986	14.33618	7.465712
2041–2070	3028	940	9.998453	21.25692	7.419244
2071–2100	2326	611	16.26631	9.887684	7.418923

Period averages of precipitation-related indicators for Tonsberg are presented in Table 8. The RX5d indicator undergoes a distinctive reduction during the 2011-2071 period but returns to the 1971-2010 levels at the end of the period. As in previous cases, both R95pTOT (contribution of very rainy days) and R99pTOT (contribution of extremely rainy days) are calculated using a five-year bootstrap period. Both of these indicators decrease rapidly after 2011 (making the 1970-2010 period into something of an outlier) with R95pTOT increasing during the second half of the century. This increase of course implies an increase in the contribution of very rainy/snowy days in the total yearly precipitation. Looking at the corresponding timeseries of yearly averages (Figures 19 and 20), the distinguishing trends of the 1970-2010 and 2071-2100 periods become evident. Comparison with other RCM simulations as well as future scenarios would be needed to evaluate the importance of these trends, which could also stem from a computational artifact of the examined simulation & emissions data.

Table 8: ETCCDI Precipitation-related Indicators for the site of Tonsberg

Period	RX5day	R95pTOT	R99pTOT
1971–2010	40	810.3914	224.6354
2011–2040	39	588.7861	177.7409
2041–2070	35	592.218	175.1839
2071–2100	47	631.9645	204.6842

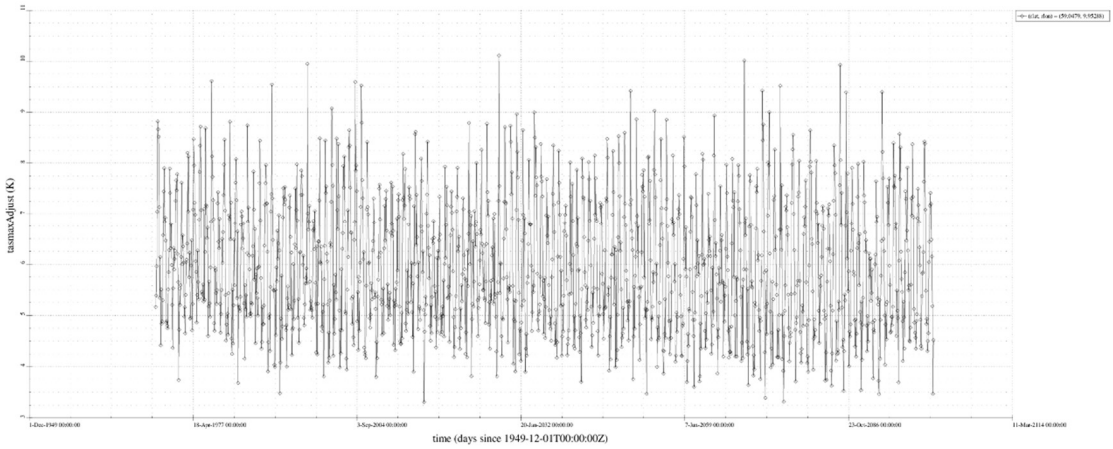

Figure 16: Time series of monthly DTR for the site of Tonsberg.

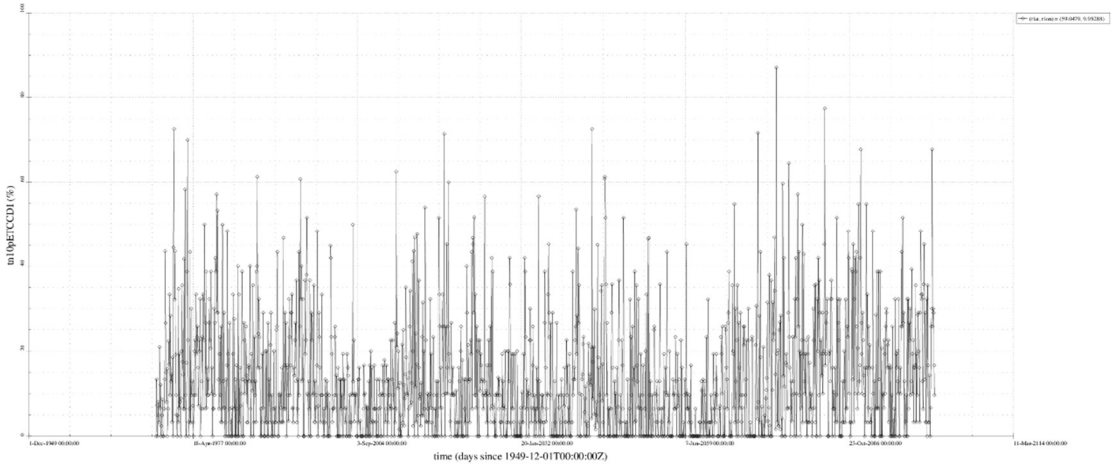

Figure 17: Time series of monthly TN10p for the site of Tonsberg.

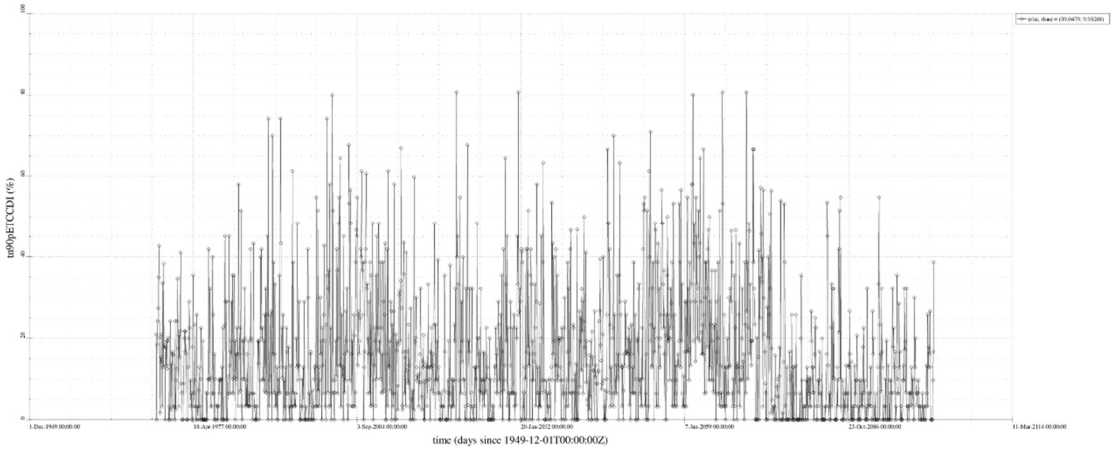

Figure 18: Time series of monthly TN90p for the site of Tonsberg.

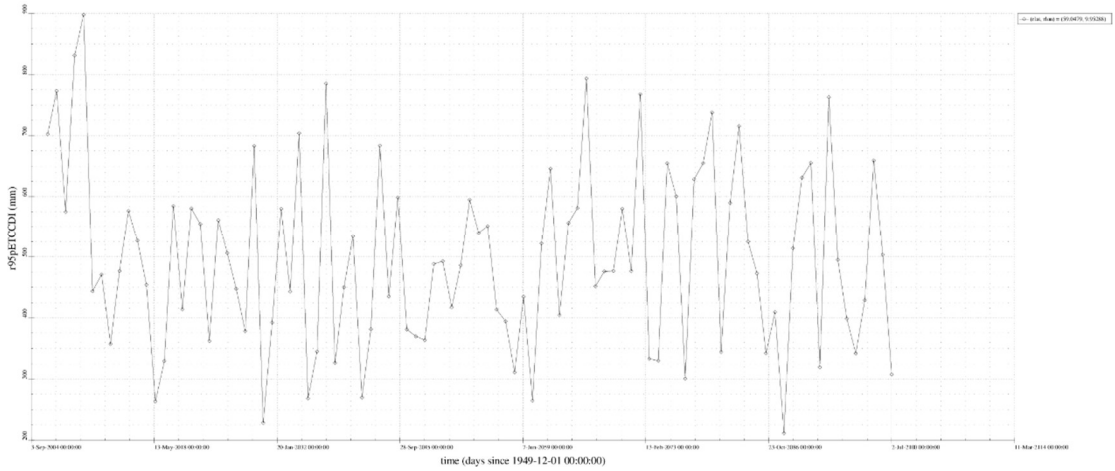

Figure 19: Time series of annual R95pTOT for the site of Tonsberg.

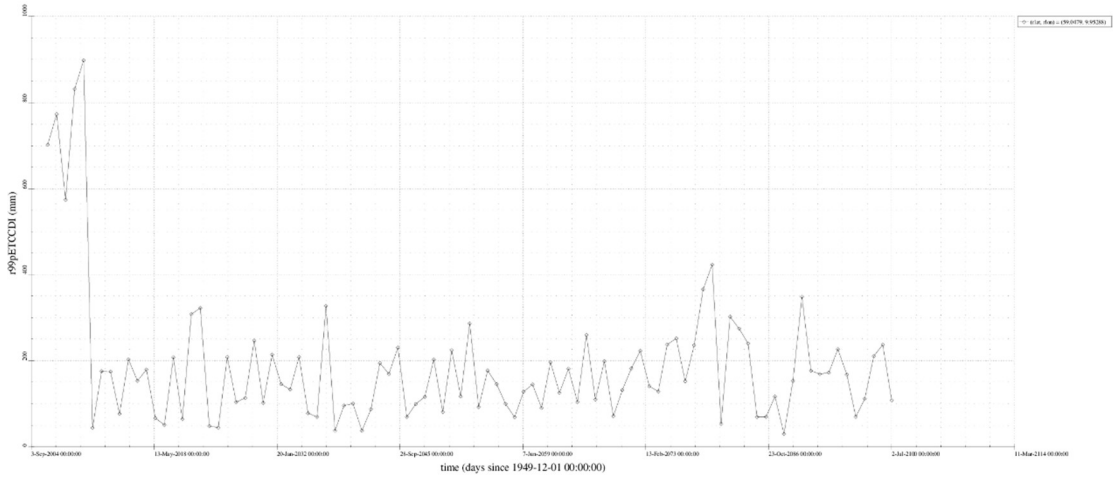

Figure 20: Time series of annual R99pTOT for the site of Tonsberg.

4. Conclusions

This document aimed to provide qualitative and quantitative assessment on the relevance of primary and secondary impact indicators derived from climate calculations based on historical data and future climatic scenarios. A set of 8 ETCCDI indices, selected to represent the most relevant atmospheric stressors for Cultural Heritage were calculated based on a GCM to RCM downscaling approach, as implemented within the EURO-CORDEX project, covering a period from 1971 to 2100. The RCP4.5 emissions scenario was used for future predictions, representing a medium-situation estimate with regards to climate change mitigation.

The meteorological indicators considered in this analysis are related to averages and extremes of ambient temperature and precipitation. The use of ETCCDI indicators, which are based on a bootstrapping methodology, ensures that secular averages and deviations thereof can be calculated by introducing the least amount of intra-annual statistical noise. Results were presented in the form of tabulated index values for four

intervals, starting from 1971 and ending to the end of the century, as well as with graphical representations of the corresponding time series.

Regarding thermal effects, the most consistend predicted trend throughout the simulation period is a decrease (down to a third, in some instances) in the number of frost days and icing days, which becomes especially pronounced in the Venice and Tonsgberg cases. This projected change would of course severely affect the freezing-thawing cycles of assets as well as the seasonal patterns of surface growths an local microflora. Nighttime temperatures are not forecasted to change significantly, although a slight increase in the percentage of cold nights is expected for Venice and Tongsberg.

For projected precipitation patterns, in most cases the relevant indicators predict little to no statistically significant change. For the case of Venice, extreme indicators show a consistent increase of very wet days and extremely wet days contribution, implying more frequent days of concentrated extreme precipitation with the associated flash-flooding risk. Tonsberg is also expected to receive increased precipitation extremes (as a fraction of precipitation total) during the second half of the century. Rhodes, on the other hand, is expected to experience less contribution from precipitation extremes during the 2071-2100 period. Together with return intervals and estimation of absolute extremes, performed elsewhere (HYPERION D3.1), these results provide strong indicators on the frequency and magnitude of effects that long-term planning should take account of.

5. References

Alexander, L.V., X. Zhang, T.C. Peterson, J. Caesar, B. Gleason, A.M.G. Klein Tank, M. Haylock, D. Collins, B. Trewin, F. Rahimzadeh, A. Tagipour, P. Ambenje, K. Rupa Kumar, J. Revadekar and G. Griffiths, 2006: Global observed changes in daily climate extremes of temperature and precipitation. *J. Geophys. Res.*, 111 (D05109), DOI:10.1029/2005JD006290.

Brink, H.W. van den and G.P. Können, 2008: The statistical distribution of meteorological outliers. *Geophys. Res. Lett.*, DOI:10.129/2008GL035967.

Coles, S.G., 2001: *An Introduction to Statistical Modeling of Extreme Values*, Springer-Verlag, London.

Dee, D. P., Uppala, S. M., Simmons, A. J., Berrisford, P., Poli, P., Kobayashi, S., Andrae, U., Balmaseda, M. A., Balsamo, G., Bauer, P., Bechtold, P., Beljaars, A. C. M., van de Berg, L., Bidlot, J., Bormann, N., Delsol, C., Dragani, R., Fuentes, M., Geer, A. J., Haimberger, L., Healy, S. B., Hersbach, H., Hólm, E. V., Isaksen, L., Kållberg, P., Köhler, M., Matricardi, M., McNally, A. P., Monge-Sanz, B. M., Morcrette, J.-J., Park, B.-K., Peubey, C., de Rosnay, P., Tavolato, C., Thépaut, J.-N., and Vitart, F. (2011), The ERA-Interim reanalysis: configuration and performance of the data assimilation system. *Quarterly Journal of the Royal Meteorological Society*, **137:** 553–597. doi:10.1002/qj.828.

Dupuis, D.J. and M. Tsao, 1998: A hybrid estimator for the Generalized Pareto and Extreme-Value Distributions. Communications in Statistics: *Theory and Methods*, 27, 925–941.

Gumbel, E.J., 1958: *Statistics of Extremes*. Columbia University Press, New York, 375pp.

Hazeleger, W., Wang, X., Severijns, C., Ştefănescu, S., Bintanja, R., Sterl, A., Wyser, K., Semmler, T., Yang, S., van den Hurk, B., van Noije, T., van der Linden, E., and van der Wiel, K. (2011), EC-Earth V2.2: description and validation of a new seamless earth system prediction model. *Climate Dynamics*, **39:** 2611–2629, doi:10.1007/s00382-011-1228-5.

Hosking, J.R.M., 1990: L-moments: Analysis and estimation of distributions using linear combinations of order statistics. *J. Roy. Stat. Soc*. (Ser. A), B52, 105–124.

Jenkinson, A. F., 1955: The frequency distribution of the annual maximum (or minimum) values of meteorological elements. *Quart. J. Roy. Meteor. Soc.*, 81, 158–171.

Katz, R.W., M.B. Parlange and P. Naveau, 2002: *Statistics of extremes in hydrology, Advances in Water Resources*, 25, 1287–1304.

Kharin, V.V. and F.W. Zwiers, 2000: Changes in the extremes in an ensemble of transient climate simulations with a coupled atmosphere–ocean GCM. *Journan of Climate*, 13, 3760–3788.

Kharin, V.V. and F.W. Zwiers, 2005: Estimating extremes in transient climate change simulations. *Journal of Climate*, 18, 1156–1173.

Kharin, V.V., F.W. Zwiers, X. Zhang and G.C. Hegerl, 2007: Changes in temperature and precipitation extremes in the IPCC ensemble of global coupled model simulations. *Journal of Climate*, 20, 1419-1444, DOI: 10.1175/JCLI4066.1

Klein Tank A.M.G., Zwiers F.W. and Zhang X., 2009. Guidelines on Analysis of extremes in a changing climate in support of informed decisions for adaptation. WMO-TD No. 1500, 56 pp.

Kotlarski, S., Keuler, K., Christensen, O. B., Colette, A., Déqué, M., Gobiet, A., Goergen, K., Jacob, D., Lüthi, D., van Meijgaard, E., Nikulin, G., Schär, C., Teichmann, C., Vautard, R., Warrach-Sagi, K., and Wulfmeyer, V. (2015), Regional climate modeling on European scales: a joint standard evaluation of the EURO-CORDEX RCM ensemble. *Geoscientific Model Developlment*, **7:** 1297–1333, doi:10.5194/gmd-7-1297-2014.

Landwehr, J.M., N.C. Matalas and J.M. Wallis, 1979: Probability weighted moments compared with some traditional techniques in estimating Gumbel parameters and quantiles. *Water Res. Research*, 15, 1055–1064.

Martin, G. M., Bellouin, N., Collins, W. J., Culverwell, I. D., Halloran, P. R., Hardiman, S. C., Hinton, T. J., Jones, C. D., McDonald, R. E., McLaren, A. J., O'Connor, F. M., Roberts, M. J., Rodriguez, J. M., Woodward, S., Best, M. J., Brooks, M. E., Brown, A. R., Butchart, N., Dearden, C., Derbyshire, S. H., Dharssi, I., Doutriaux-Boucher, M., Edwards, J. M., Falloon, P. D., Gedney, N., Gray, L. J., Hewitt, H. T., Hobson, M., Huddleston, M. R., Hughes, J., Ineson, S., Ingram, W. J., James, P. M., Johns, T. C., Johnson, C. E., Jones, A., Jones, C. P., Joshi, M. M., Keen, A. B., Liddicoat, S., Lock, A. P., Maidens, A. V., Manners, J. C., Milton, S. F., Rae, J. G. L., Ridley, J. K., Sellar, A., Senior, C. A., Totterdell, I. J., Verhoef, A., Vidale, P. L., and Wiltshire, A. (2011), The HadGEM2 family of Met Office Unified Model climate configurations. *Geoscientific Model Developlment*,**4:** 723–757, doi:10.5194/gmd-4-723-2011.

Peterson, T.C. and M.J. Manton, 2008: *Monitoring changes in climate extremes – A tale of international collaboration*. BAMS, DOI:10.1175/2008BAMS2501.1.

Smith, R.L., 2002: *Statistics of extremes with applications in environment, insurance and finance*. http://www.stat.unc.edu/postscript/rs/semstatrls.pdf

Stevens, B., Giorgetta, M., Esch, M., Mauritsen, T., Crueger, T., Rast, S., Salzmann, M.m Schmidt, H., Bader, J., Block, K., Brokopf, R., Fast, I., Kinne, S., Kornblueh, L., Lohmann, U., Pincus, R., Reichler, T., and Roeckner, E. (2013), Atmospheric component of the MPI-M Earth System Model: ECHAM6. *Journal of Advances in Modeling Earth Systems*, 5**:** 146–172, doi:10.1002/jame.20015.

van Vuuren, D. P., Edmonds, J., Kainuma, M., Riahi, K., Thomson, A., Hibbard, K., Hurtt, G. C., Kram, T., Krey, V., Lamarque, J.-F., Masui, T., Meinshausen, M., Nakicenovic, N., Smith, S. J., and Rose, S. K. (2011), The representative concetration pathways: an overview. *Climatic Change*, 109: 5–31, doi:10.1007/s1+584-011-0148-z.

WMO, 1989: *Statistical Distributions for Flood Frequency Analysis*. WMO-No. 718 and Operational Hydrology Report No. 33.

Zhang, X., G. Hegerl, F.W. Zwiers and J. Kenyon, 2005: Avoiding inhomogeneity in percentile-based indices of temperature extremes, *J. Clim.*, 18, 1641–1651.

URL1: http://www.clivar.org/organization/etccdi/etccdi.php